

# Regular motions in double bars.

## I. Double-frequency orbits and loops

Witold Maciejewski<sup>1,2\*</sup> and E. Athanassoula<sup>2</sup>

<sup>1</sup>*Astrophysics Research Institute, Liverpool John Moores University, Twelve Quays House, Egerton Wharf, Birkenhead, CH41 1LD*

<sup>2</sup>*LAM, Observatoire Astronomique de Marseille Provence, CNRS, 2 Place Le Verrier, F-13248 Marseille Cedex 4, France*

2 December 2018

### ABSTRACT

Bars in galaxies are mainly supported by particles trapped around stable periodic orbits. These orbits represent oscillatory motion with only one frequency, which is the bar driving frequency, and miss free oscillations. We show that a similar situation takes place in double bars: particles get trapped around parent orbits, which in this case represent oscillatory motion with two frequencies of driving by the two bars, and which also lack free oscillations. Thus the parent orbits, which constitute the backbone of an oscillating potential of two independently rotating bars, are the double-frequency orbits. These orbits do not close in any reference frame, but they map onto loops, first introduced by Maciejewski & Sparke (1997). Trajectories trapped around the parent double-frequency orbit map onto a set of points confined within a ring surrounding the loop.

**Key words:** methods: analytical — stellar dynamics — galaxies: kinematics and dynamics — galaxies: nuclei — galaxies: spiral — galaxies: structure

## 1 INTRODUCTION

Double bars in galaxies, also called nested bars or bars within bars, are systems with a nuclear bar embedded within a large-scale outer bar. Such systems appear to be common in galaxies: recent surveys show that up to 30% of early-type barred galaxies contain them (Erwin & Sparke 2002), and they are also present in galaxies of types as late as Sbc and Sc (Laine et al. 2002). At least 50 double-barred systems are now known (Erwin 2004). The relative orientation of the two bars is random (Buta & Crocker 1993; Friedli & Martinet 1993; Wozniak et al. 1995; Erwin & Sparke 2002; Laine et al. 2002), which is expected if the bars were to rotate with different pattern speeds. Inner bars, like large bars, are made of relatively old stellar populations, since they remain distinct in near infrared (Friedli et al. 1996).

Orbits in galaxies with two independently rotating bars do not conserve the Jacobi integral, and it is a complex dynamical task to explain how such systems are sustained. This task has been approached with  $N$ -body simulations (e.g. Friedli & Martinet 1993; Rautiainen, Salo & Laurikainen 2002; Debattista & Shen 2007; Heller, Shlosman & Athanassoula 2007), and through studies of trajectories with a selected set of initial conditions (El Zant & Shlosman 2002). Nested bars influence each other throughout their extent: they can change shapes and accelerate as they rotate through each other (Maciejewski & Sparke 2000), and the orbital structure of the outer bar can be significantly modified by the inner bar, especially near its corotation. In general, the piling up of resonances

created by each bar may lead to considerable chaotic zones, and, if the fraction of chaotic orbits in double bars were large, such systems should not last for long time periods. Long-lasting double bars should therefore have a substantial fraction of regular orbits, and one should be able to describe their dynamics by means similar to those invoked in the case of single bars, *i.e.* in terms of the regular orbits that they admit. Such an approach was originally proposed by Maciejewski & Sparke (1997, 2000). In this paper we propose that the backbone of the oscillating potential of double bars is made of double-frequency orbits, and we explicitly show that these orbits map onto the loops invented by Maciejewski & Sparke.

In Section 2, we outline in more detail the approach proposed in this paper. In Section 3, we use the epicyclic approximation to show that two frequencies on an orbit in the plane of an oscillating potential of a doubly barred galaxy are indispensable. We also show there that double-frequency orbits map onto loops in the epicyclic approximation. In Section 4, we analyze particle trajectories in double bars in the general non-linear case. We develop a method of analysis in Fourier space that allows us to distinguish regular trajectories from chaotic ones, and to recover the three fundamental frequencies of the regular orbits. We find that in the general, non-linear case double-frequency orbits map onto loops as well, and that they can trap around themselves regular orbits.

## 2 CONCEPTUAL OUTLINE

Particle motion in a potential of double bars belongs to the general problem of motion in an oscillating potential (Louis & Ger-

\* E-mail: witold@astro.ox.ac.uk

hard 1989; Sridhar 1989). In this particular case, the potential oscillates with the relative period of the bars. The best known example of the general problem of motion in an oscillating potential is the restricted elliptical 3-body problem. Families of closed periodic orbits have been found in this last problem, where the test particle moves in the potential of a binary star with components on elliptical orbits (*e.g.* Broucke 1969). Such families, however, are parametrized by values that also characterize the potential (i.e. ellipticity of the stellar orbit and the mass ratio of the stars), and the orbital periods there are commensurate with the oscillation period of the potential. For a given potential, these families are reduced to single orbits separated in phase-space. The solution for double bars is formally identical, and there an orbit can close only when the orbital period is commensurate with the relative period of the bars. Howard (1994) found such periodic orbits in double bars with periods equal to a multiplicity of the bars' relative period. Such orbits are separated in phase-space and therefore families of closed periodic orbits are not sufficient to provide orbital support for nested bars.

Binney & Spergel (1982, 1984) developed a formalism that classifies the orbits based on the frequencies at which they oscillate. The Fourier transform of any dynamical variable on a regular orbit (position, velocity) should return a line spectrum. Regular orbits in the plane of a stationary galaxy correspond to oscillations with two frequencies: the angular frequency, and the epicyclic frequency – the orbit's fundamental frequency. Closed periodic orbits are a particular case of regular orbits. They oscillate with one frequency only, whose inverse is the period of the orbit. In general, a single frequency in the system may appear when the two frequencies above are commensurate, or when oscillations with one of the frequencies are missing. A rotating asymmetry (*e.g.* a bar) in the system constitutes a periodic driving force. As in the case of a driven harmonic oscillator, the orbits always respond to this driving force by oscillations with the frequency of the driver. These oscillations are always present, and if the orbit is to close in the frame rotating with the bar, they must be the only oscillations, i.e. the free oscillations with the epicyclic frequency must be absent.

The oscillating potential of double bars changes periodically with the relative period of the bars. Since a Hamiltonian system in  $N$  dimensions with a periodically varying potential is equivalent to an autonomous system in  $N + 1$  dimensions (see *e.g.* Lichtenberg & Lieberman 1992, Louis & Gerhard 1988), regular motions in the plane of a doubly barred galaxy should correspond to oscillations with three frequencies. As before, Fourier analysis of a closed periodic orbit will return only one frequency. Aside from oscillations with three frequencies, and with one frequency only, there remain oscillations with two frequencies. Since two bars in a doubly barred galaxy constitute two periodic driving forces, oscillations with two frequencies should characterize response of the system to this periodic driving, when free oscillations are absent. Thus, the role of double-frequency orbits in double bars should be equivalent to the role of closed periodic orbits in a single bar. In the unchanging potential of a single bar, regular orbits are trapped around stable closed periodic orbits, which constitute the backbone of that potential. Here we postulate that stable double-frequency orbits constitute the backbone of an oscillating potential of double bars, and trap around themselves regular orbits with the maximum number of frequencies, which, in this case, is three.

The approach outlined above indicates that oscillating potentials can be supported by orbits that do not have to be closed and periodic. With this approach we overcome the problem of scarcity of closed periodic orbits that hampered previous searches for sup-

port of oscillating potentials. The concept of closed periodic orbit is too limiting for the investigation of oscillating systems, and we replace it by another, broader description of particle motion, which still captures its regularities. Our description, based on double-frequency orbits which are not closed and periodic, can provide the backbone of an oscillating system for the same reason for which closed periodic orbits in stationary potentials do, and account for longevity of double bars.

Double-frequency orbits are difficult to visualize, because they do not close in any reference frame. However, in this paper we will show that they can be mapped onto closed curves, which are much easier to visualize. The mapping is done by recording the position of a particle on a double-frequency orbit at every consecutive alignment of the bars. Thus particle's position is written only when the oscillating galaxy periodically regains one specified shape. In this paper we show that positions of particles on a double-frequency orbit recorded at every consecutive alignment of the bars populate a closed curve. By construction, this curve transforms into itself at each consecutive alignment of the bars. Thus a set of particles populating such a curve oscillates periodically with the oscillating potential. Maciejewski & Sparke (1997) discovered such curves in a potential with a double bar, and they called them loops. Loops can be used as a convenient descriptor of orbital structure in an oscillating potential. Like closed periodic orbits in stationary potentials, they can indicate the zones that can be supported by regular motions. In the remaining sections we will show that double-frequency orbits can form the backbone of oscillating potentials, and that loops make a unique tool for studying such orbits.

### 3 THE EPICYCLIC SOLUTION

#### 3.1 The general epicyclic solution for any number of bars

If a galaxy has a bar that rotates with a constant pattern speed, it is convenient to study particle orbits in the reference frame rotating with the bar. If two or more bars are present and each rotates with its own pattern speed, there is no reference frame in which the potential remains unchanged. In order to point out formal similarities in solutions for one and many bars, we solve the linearized equations of motion in the inertial frame. As we show below, this is equivalent to the solution in any rotating frame and the transformation is particularly simple: in the rotating frame the centrifugal and Coriolis terms are equivalent to the Doppler shift of the angular velocity.

In a frame rotating with a constant pattern speed  $\Omega_B$ , the equation of motion of a particle in a potential  $\Phi$  can be written as

$$\ddot{\mathbf{r}}' = -\nabla\Phi - 2(\boldsymbol{\Omega}_B \times \dot{\mathbf{r}}') - \boldsymbol{\Omega}_B \times (\boldsymbol{\Omega}_B \times \mathbf{r}'),$$

where the position of the particle in the rotating frame is indexed by prime. In polar coordinates in the plane of the galactic disc, its  $R'$  and  $\varphi'$  components are

$$\ddot{R}' - R'(\dot{\varphi}' + \Omega_B)^2 = -\frac{\partial\Phi}{\partial R}, \quad (1)$$

$$R'\ddot{\varphi}' + 2\dot{R}'(\dot{\varphi}' + \Omega_B) = -\frac{1}{R}\frac{\partial\Phi}{\partial\varphi}. \quad (2)$$

Since the angular velocity  $\dot{\varphi}'$  in the rotating frame is related to the angular velocity  $\dot{\varphi}$  in the inertial frame by

$$\dot{\varphi} = \dot{\varphi}' + \Omega_B,$$

and radial coordinates in both frames are equal ( $R = R'$ ), equa-

tions (1) and (2) in the inertial frame take the form

$$\ddot{R} - R\dot{\varphi}^2 = -\frac{\partial\Phi}{\partial R}, \quad (3)$$

$$R\ddot{\varphi} + 2\dot{R}\dot{\varphi} = -\frac{1}{R}\frac{\partial\Phi}{\partial\varphi}, \quad (4)$$

which are the  $R$  and  $\varphi$  components of the equation of motion in the inertial frame:

$$\ddot{\mathbf{r}} = -\nabla\Phi.$$

This equivalence remains true when vertical motion is included in three dimensions. For the rest of this section we adopt the inertial frame, in which the  $R$  and  $\varphi$  components of the equation of motion take a particularly simple form of (3, 4).

We want to linearize equations (3) and (4) for departures from circular motion in a nearly axisymmetric potential. We thus perform two expansions simultaneously. One is a linearization of the quantities describing the motion by their expansion to first-order terms in  $R - R_0$ , where  $R_0$  is the radius of the circular orbit in the axisymmetric potential. The other is expansion of the potential in a Fourier series, with the zeroth-order term being the axisymmetric component. In both expansions, zeroth-order terms are indexed with 0 and first-order terms are indexed with  $I$ . These expansions can be written as

$$R(t) = R_0 + R_I(t), \quad (5)$$

$$\varphi(t) = \varphi_{00} + \Omega_0 t + \varphi_I(t), \quad (6)$$

$$\Phi(R, \varphi, t) = \Phi_0(R) + \Phi_I(R, \varphi, t), \quad (7)$$

where second- and higher-order terms are neglected. In the inertial frame, the angle coordinate  $\varphi$  of a particle in the zeroth approximation is  $\varphi_0 = \varphi_{00} + \Omega_0 t$ , where  $\varphi_{00}$  is the value of  $\varphi_0$  at  $t = 0$ , and where the angular velocity  $\Omega_0$  on the circular orbit of radius  $R_0$  relates to the potential  $\Phi_0$  through the zeroth order of (3):  $\Omega_0^2 = (1/R_0)(\partial\Phi_0/\partial R)|_{R_0}$ . The zeroth order of (4) is identically equal to zero. In the zeroth order approximation, the axisymmetric part of the potential,  $\Phi_0$ , is time-independent. The first order term  $\Phi_I$ , describing asymmetry in the potential, may depend on time.

In the expansion defined above, the first order parts of (3) and (4) take respectively the forms

$$\ddot{R}_I - 4A\Omega_0 R_I - 2R_0\Omega_0\dot{\varphi}_I = -\frac{\partial\Phi_I}{\partial R}|_{R_0, \varphi_0}, \quad (8)$$

$$R_0\ddot{\varphi}_I + 2\Omega_0\dot{R}_I = -\frac{1}{R_0}\frac{\partial\Phi_I}{\partial\varphi}|_{R_0, \varphi_0}, \quad (9)$$

where  $A$  is the Oort constant defined by  $4A\Omega_0 = \Omega_0^2 - \frac{\partial^2\Phi_0}{\partial R^2}|_{R_0}$ .

Furthermore, we assume that, to the first order, the departure of the barred potential from axial symmetry can be described by a term  $\cos(2\varphi)$ . If  $N$  bars, indexed by  $i$ , rotate independently as solid bodies with angular velocities  $\Omega_i$ , the time-dependent first-order correction  $\Phi_I$  to the potential can be written as

$$\Phi_I(R, \varphi, t) = \sum_i^N \Psi_i(R) \cos[2(\varphi - \Omega_i t)], \quad (10)$$

where the radial dependence  $\Psi_i(R)$  has been separated from the angular dependence. The lack of phase in the above trigonometric functions means that we define as  $t = 0$  the time when all the bars are aligned. Derivatives of (10) enter the right-hand sides of (8) and (9), which after introducing

$$\omega_i = 2(\Omega_0 - \Omega_i), \quad (11)$$

take the form

$$-\ddot{R}_I + 4A\Omega_0 R_I + 2R_0\Omega_0\dot{\varphi}_I = \sum_i^N \frac{\partial\Psi_i}{\partial R}|_{R_0} \cos(\omega_i t + 2\varphi_{00}) \quad (12)$$

$$R_0\ddot{\varphi}_I + 2\Omega_0\dot{R}_I = \frac{2}{R_0} \sum_i^N \Psi_i(R_0) \sin(\omega_i t + 2\varphi_{00}). \quad (13)$$

In order to solve the set of equations (12,13), one can integrate (13) and get an expression for  $R_0\dot{\varphi}_I$ , which furthermore can be substituted into (12). This substitution eliminates  $\varphi_I$ , and one gets a single second order equation for  $R_I$ , which can be written schematically as

$$\ddot{R}_I + \kappa_0^2 R_I = \sum_i^N M_i \cos(\omega_i t + 2\varphi_{00}) + C_\varphi, \quad (14)$$

where  $M_i = -\frac{4\Omega_0\Psi_i}{\omega_i R_0} - \frac{\partial\Psi_i}{\partial R}|_{R_0}$ ,  $\kappa_0^2 = 4\Omega_0(\Omega_0 - A)$ , and  $C_\varphi/2\Omega_0$  is the integration constant that appears after integrating (13). Below, we will show that  $C_\varphi$  can be removed by redefining the guiding radius. What is left of (14), is the equation of a harmonic oscillator with multiple driving terms. Thus in the linear approximation, the orbital motion of a particle in the potential of rotating bars is equivalent to the motion of a driven harmonic oscillator. The general solution of (14) is well known and can be written as

$$R_I(t) = C_1 \cos(\kappa_0 t + \delta) + \sum_i^N P_i \cos(\omega_i t + 2\varphi_{00}) + C_\varphi/\kappa_0^2, \quad (15)$$

where the coefficients  $P_i$  are functions of  $M_i$ . The first term in the right hand side of (15) is the solution of the homogeneous part of (14), and it corresponds to a free oscillation with the local epicyclic frequency  $\kappa_0$  around the circular orbit in the axisymmetric potential. The coefficient  $C_1$  is unconstrained. The terms in the sum over  $i$  in (15) are the particular solutions of the inhomogeneous equation (14), and they describe oscillations driven by the bars. Note that the frequency of the driving force (shifted to the frame of the rotating guiding centre) is always present in the oscillations. Thus, orbits in potentials with  $N$  independently rotating bars will oscillate with at least  $N$  frequencies, unless the shifted frequencies are commensurate.

The formula for  $\varphi_I(t)$  can be obtained by substituting (15) into the time-integrated (13). As a result, one gets

$$\varphi_I = C_2 \cos(\kappa_0 t + \delta) + \sum_i^N Q_i \cos(\omega_i t + 2\varphi_{00}) - \frac{2AC_\varphi}{\kappa_0^2 R_0}, \quad (16)$$

where again  $C_2$  is unconstrained and the  $Q_i$  are determined by the coefficients of the equations above. Note that the integration constant  $C_\varphi/\kappa_0^2$  in (15) can be incorporated into  $R_0$  in (5), giving the new guiding radius  $R_0 + C_\varphi/\kappa_0^2$ . Since  $A = -\frac{1}{2}R_0\frac{d\Omega_0}{dR}|_{R_0}$ , expanding  $\Omega$  to the first order gives the angular velocity at this new radius

$$\Omega_0|_{R_0 + C_\varphi/\kappa_0^2} = \Omega_0|_{R_0} + \frac{C_\varphi}{\kappa_0^2} \frac{d\Omega_0}{dR}|_{R_0} = \Omega_0|_{R_0} - \frac{2AC_\varphi}{\kappa_0^2 R_0}.$$

Thus the integration constant  $-\frac{2AC_\varphi}{\kappa_0^2 R_0}$  in (16) represents the correction to the zeroth order angular velocity  $\Omega_0$  incurred by a change of the guiding radius  $R_0$  by  $C_\varphi/\kappa_0^2$ , which is the integration constant in (15). Hence both integration constants can be incorporated by modifying the guiding radius in the epicyclic approximation. Eventually, in the epicyclic approximation, the most general solution for particle motion in the symmetry plane of a potential with  $N$  independently rotating bars is

$$R_I(t) = C_1 \cos(\kappa_0 t + \delta) + \sum_i^N P_i \cos(\omega_i t + 2\varphi_{00}), \quad (17)$$

$$\varphi_I(t) = \frac{C_2}{\kappa_0} \sin(\kappa_0 t + \delta) + \sum_i^N \frac{Q_i}{\omega_i} \sin(\omega_i t + 2\varphi_{00}) + \text{const}, \quad (18)$$

where  $R_I$  and  $\varphi_I$  are polar coordinates in the inertial frame. The integration constant in (18) is an unconstrained parameter. From (17) and (18) one can see that up to  $N + 1$  independent frequencies are present in this motion.

### 3.2 Closed periodic orbits in a single bar

In a potential with a single bar there is only one term in the sums over  $i$  in (17) and (18). Therefore in general two frequencies are present in orbital motion, as expected for motion in a symmetry plane of a static potential. However, closed periodic orbits have only one frequency. Oscillations with the frequency of the rotating bar (corrected for the angular frequency of the guiding centre) are always present in orbital motion, analogously to oscillations with the frequency of the driving force in a driven harmonic oscillator. The linear approximation breaks down when the frequency of free oscillations becomes commensurate with the frequency of the driving force. Therefore, in this framework, in order for the orbits to close, the amplitude of free oscillations with frequency  $\kappa_0$  has to be zero. For  $C_1 = C_2 = 0$  and  $N = 1$ , equations (17) and (18) describe closed periodic orbits in the linearized problem of a particle motion in a single bar.

Consider, for the case where free oscillations are absent, the change in the values of  $R_I$  and  $\varphi_I$  after the particle's guiding centre returns to its starting point in the frame corotating with the bar. This happens after time period  $2\pi/(\Omega_0 - \Omega_1)$ . Replacing  $t$  by  $t + 2\pi/(\Omega_0 - \Omega_1)$  leads to

$$\begin{aligned} R_I &= P_1 \cos\left[\omega_1\left(t + \frac{2\pi}{\Omega_0 - \Omega_1}\right) + 2\varphi_{00}\right] \\ &= P_1 \cos(\omega_1 t + 4\pi + 2\varphi_{00}). \end{aligned}$$

Thus, after time  $2\pi/(\Omega_0 - \Omega_1)$  the solution for  $R_I$  returns to its starting value. The same holds true for  $\varphi_I$  and the orbit closes in the bar frame. Thus,  $2\pi/(\Omega_0 - \Omega_1)$  is the full period of this particle.

### 3.3 Closed periodic orbits in double bars

While the potential of a single bar is stationary in the bar's frame, that of a galaxy with two independently rotating bars is not stationary in any reference frame. For two bars there are two terms in the sums over  $i$  in (17) and (18), and therefore even if the amplitude of free oscillations with the frequency  $\kappa_0$  is zero, two frequencies are present in the orbital motion. They are the frequencies of the driving forces imposed by the two tumbling bars, and oscillations with these two frequencies have always non-zero amplitude. Orbits with two frequencies do not close, therefore closed periodic orbits should not be the fundamental orbits in double bars.

However, closed periodic orbits do exist in double bars, and in the linear approximation this happens when the frequencies in the sums over  $i$  in (17) and (18) are commensurate, *i.e.* when  $n\omega_1 = m\omega_2$  for  $n, m$  integer. In that case there is effectively only one independent frequency and the orbit closes. However, this happens only for a discrete set of values of the angular velocity of the guiding centre

$$\Omega = \frac{m\Omega_1 - n\Omega_2}{m - n}. \quad (19)$$

Therefore in the epicyclic approximation there is an infinity of closed periodic orbits in double bars, but these orbits do not form families continuous with the radius of the guiding centre. Although formally any orbit in double bars, which responds to two driving forces by oscillating with two frequencies, can be approximated by a closed periodic orbit of angular frequency (19), such an orbit closes after very many bar periods, and describing motions in double bars in terms of such closed periodic orbits is not very convenient. Moreover, although any orbit oscillating with two frequencies has a closed periodic orbit in its infinitesimal vicinity with sufficiently large  $m$  and  $n$ , such a closed periodic orbit cannot be considered to be a parent orbit, because orbits with two independent frequencies are not constituted by free oscillations around that orbit. Finally, in the non-linear regime, Howard (1994) found that closed periodic orbits in doubly barred potentials, with periods predicted by (19) are often unstable, and therefore they cannot serve as parent orbits. Thus, closed periodic orbits are unlikely to provide sufficient backbone supporting double bars. Below we present a more convenient way serving this purpose.

### 3.4 Double-frequency orbits in double bars. Loops

In Sect.3.2 we showed that in the case of a single bar, when there are no free oscillations, the linear solution (17) and (18) returns only one oscillation frequency, which indicates a closed periodic orbit. In a solution for double bars, two independent frequencies are present in general, hence one should expect that *double-frequency* orbits take place of closed periodic orbits there. Such orbits do not close in any reference frame, because when a term from one bar in (17) and (18) returns to its initial value, the term from the other bar does not.

However, consider the change in value of  $R_I$  and  $\varphi_I$  after time  $\pi/(\Omega_2 - \Omega_1)$ , which is the relative period of the bars. Every such time interval, the mass distribution in the galaxy and its potential are the same in the frame rotating with either bar. With amplitudes of free oscillations in (17) set to zero one gets

$$\begin{aligned} R_I &= P_1 \cos\left[\omega_1\left(t + \frac{\pi}{\Omega_2 - \Omega_1}\right) + 2\varphi_{00}\right] \\ &+ P_2 \cos\left[\omega_2\left(t + \frac{\pi}{\Omega_2 - \Omega_1}\right) + 2\varphi_{00}\right] \\ &= P_1 \cos\left(\omega_1 t + 2\pi \frac{\Omega_0 - \Omega_1}{\Omega_2 - \Omega_1} + 2\varphi_{00}\right) \\ &+ P_2 \cos\left(\omega_2 t + 2\pi \frac{\Omega_0 - \Omega_2}{\Omega_2 - \Omega_1} + 2\varphi_{00}\right) \\ &= P_1 \cos(\omega_1 t + 2\pi + 2\varphi_{01}) + P_2 \cos(\omega_2 t + 2\varphi_{01}), \end{aligned}$$

where  $\varphi_{01} = \varphi_{00} + \pi \frac{\Omega_0 - \Omega_2}{\Omega_2 - \Omega_1}$ . The same result can be obtained for  $\varphi_I$ . This means that the time transformation  $t \rightarrow t + \pi/(\Omega_2 - \Omega_1)$  is equivalent to the change in the starting position angle of a particle from  $\varphi_{00}$  to  $\varphi_{01}$ . Consider the motion of a set of particles that have the same guiding radius  $R_0$ , but start at various position angles  $\varphi_{00}$ . This is a one-parameter set, therefore in the disc plane it is represented by a curve, and because of continuity of (17) and (18) and their periodicity at a fixed  $t$ , this curve is closed. After time  $\pi/(\Omega_2 - \Omega_1)$ , a particle starting at angle  $\varphi_{00}$  will take the place of the particle which started at  $\varphi_{01}$ , a particle starting at  $\varphi_{01}$  will take the place of another particle from this curve and so on. The whole curve will regain its shape and position every  $\pi/(\Omega_2 - \Omega_1)$  time interval, although positions of particles on the curve will shift. This

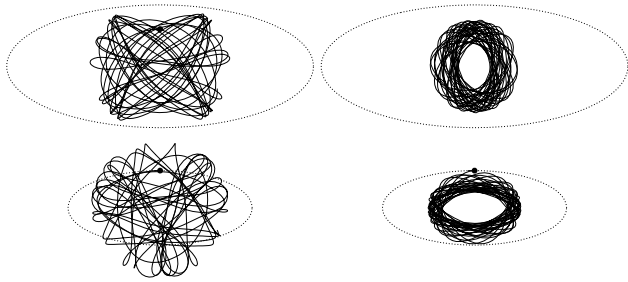


**Figure 1.** Two example trajectories (one in the two left panels, one in the two right ones) of a particle that moves in the potential of two independently rotating bars from Model 1 of Maciejewski & Sparke (2000). Large dots mark the starting position of the particle at 1.7-kpc distance from the centre of the galaxy, on the minor axis of the bars, at the moment when the corresponding axes of both bars overlap. The initial particle’s velocity vector is in both examples perpendicular to the minor axis, and its value equal to  $v_x = 220 \text{ km s}^{-1}$  (left panels) and  $v_x = 150 \text{ km s}^{-1}$  (right panels). The particle is followed for 10 relative periods of the bars, and its trajectory is displayed in the frame corotating with the big, outer bar (top panels); and with the small, inner bar (bottom panels). Each bar is outlined in its own reference frame by a dotted line.

curve is the epicyclic approximation to the *loop* introduced by Maciejewski & Sparke (1997, 2000): a curve made of particles moving in a given potential, such that the curve returns periodically to its original shape and position. In the case of two bars, the period is the relative period of the bars, and in the epicyclic approximation the loop is made out of particles having the same guiding radius  $R_0$ . Particles on the loop respond to the periodic driving force from the two bars, but they lack any free oscillations. Note that the appearance of the loops is the same, no matter which bar’s reference frame is used. Thus, loops are a convenient descriptor of orbital structure in an oscillating potential. An example of a set of loops in a doubly barred galaxy in the epicyclic approximation was given by Maciejewski & Sparke (1997). The loops occupy there a significant part of the disc.

Note that the linear solution presented here gives a prescription for constructing a loop in a general case as well. If a particle is on a double-frequency orbit, then the loop onto which the orbit maps can be constructed by registering the position of the particle every relative period of the bars, until the whole  $2\pi$  range of angular coordinates is densely populated. However, this construction requires following the particle for many relative periods of the bars, hence it will likely recover loops that are maps of stable double-frequency orbits only.

## 4 FULL NONLINEAR SOLUTION FOR PARTICLE MOTION IN NESTED BARS

### 4.1 Three types of trajectories

Tools and concepts useful in the search for ordered motions in double bars are best introduced through the inspection of particle trajectories in such systems. We use the potential of Model 1 defined in Maciejewski & Sparke (2000), so that our results can be directly compared to the results there. In order to describe gravitational potential in their models, Maciejewski & Sparke use the analytical formulae originally proposed by Athanassoula (1992). The formulae comprise the modified Hubble profile representing the bulge, the Kuzmin-Toomre profile representing the disc, and the Ferrers

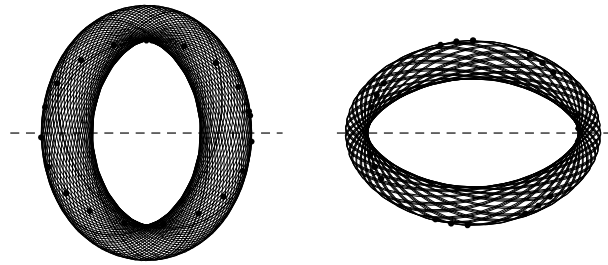


**Figure 2.** Most regular trajectory that starts at 1.7-kpc distance from the centre of the doubly barred potential from Model 1 of Maciejewski & Sparke (2000), followed for 20 relative periods of the bars, and written in the frame corotating with the big bar (left), and with the small bar (right). The major axis of each bar in its own reference frame is marked by the dashed line. Dots mark positions of the particle at every alignment of the bars (see Sect.4.4).

formula describing each bar. The exponent in the Ferrers formula is 2. In Model 1 of Maciejewski & Sparke, the outer, main bar is 7 kpc long, and the inner bar is 60% in size of the outer one. The axial ratio of each bar is 2.5. The quadrupole moment of the outer bar is only  $2.25 \times 10^{10} M_\odot \text{ kpc}^2$  in Model 1, and the mass of the inner bar is 60% of that of the outer one, hence both bars in this model are rather weak. Pattern speeds of the bars are not commensurate ( $\Omega_1 = 24.03 \text{ km s}^{-1} \text{ kpc}^{-1}$ ,  $\Omega_2 = 41.90 \text{ km s}^{-1} \text{ kpc}^{-1}$ ), and indicate rapidly rotating bars: the corotation radius of each bar is about 20% larger than its semi-major axis. The Inner Lindblad Resonance of the outer bar is located at 2.9 kpc, hence there is no resonant coupling between the bars in this model.

Consider a particle moving in this potential inside the corotation of the inner bar. Simple experiments exploring a limited range of initial conditions – with the particle starting on the minor axis of the bars at the moment when the axes overlap and with velocity vector perpendicular to that axis – show that if the initial velocity is small enough, the particle usually remains bound. Its trajectory may look regular or irregular. To illustrate this, in Figures 1 and 2 we present three trajectories of a particle starting at 1.7-kpc distance from the centre of the galaxy with three different initial velocities. A typical irregular trajectory is shown in the left panels of Fig.1 (starting velocity  $v_x = 220 \text{ km s}^{-1}$ ). Since the trajectory depends on the reference frame, it is plotted twice, once for the reference frame of each bar. However, particle trajectories usually look more regular: an example is given in the right panels of Fig.1 (starting velocity  $v_x = 150 \text{ km s}^{-1}$ ). These trajectories look like if they were trapped around some stable regular orbit.

Fine adjustments of the initial velocity lead to a highly harmonious trajectory (Fig.2, starting velocity  $v_x = 180 \text{ km s}^{-1}$ ), which appears even more regular than the trajectory from the right panels of Fig.1. Moreover, this is the most regular trajectory that we can find by varying the initial velocity. In particular, we do not find any closed periodic orbits that this trajectory can be related to. Below we will formalize the meaning of being ‘most regular’ in this context. The trajectory from Fig.2 looks like a loop orbit in a potential of a single bar<sup>1</sup> (see e.g. fig.3.7a in Binney & Tremaine 1987). In Sect.4.2, we will show that this morphological similarity

<sup>1</sup> in the existing nomenclature, which we continue to use, a loop orbit is an orbit in a time-independent potential, and it has no relation to a loop, which is a map of a double-frequency orbit in a time-dependent oscillating potential

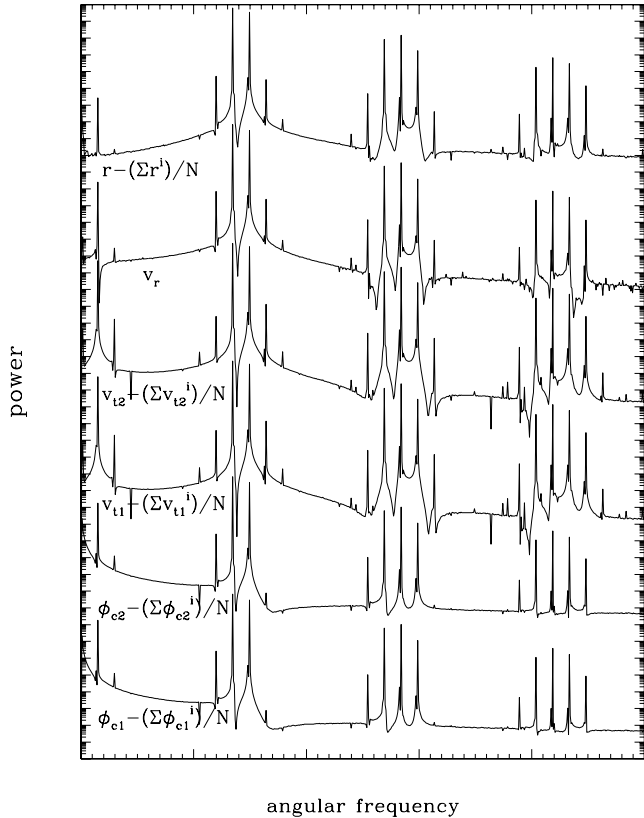


**Figure 3.** One-sided power spectral density (power spectra) from fast Fourier transform of all six dynamical variables described in the text on an exemplary regular trajectory. The vertical axis is logarithmic, with the value increasing by one order of magnitude every large tick mark. For clarity, the spectra are shifted in power from their neighbours by 7 large tick marks each.

occurs because in both cases orbital oscillations with two frequencies are involved. The loop orbit in a single bar forms when a particle oscillates around a closed periodic orbit. Therefore, it involves two frequencies: the frequency of the free oscillation, and the frequency of driving by the bar. In Sect.4.2.1 we will demonstrate that in the trajectory from Fig.2, the two frequencies are the frequencies of driving by the two bars, while the free oscillation is absent. This is the reason why the trajectory from Fig.2 appears most regular: adding the free oscillation with its own frequency will make the appearance of the trajectory less regular.

## 4.2 Orbital frequencies

In order to see what frequencies are present in the motion of a particle on a given trajectory, we Fourier-analyse any dynamical variable on this trajectory. Fast Fourier transform method has been employed, and the trajectory was traced for 100 alignments of the bars, with dynamical variables sampled  $N = 2^{13}$  times at equal time intervals. We transformed the polar coordinates of the particle, as well as its polar velocity components. The values of the radial velocity  $v_r$  entered the transformation directly, while the radial coordinate  $r$  had its average over  $N$  samplings subtracted before it was transformed. Similarly, the average over  $N$  samplings of the tangential velocity  $v_t$  was subtracted from its values before they entered the Fourier transform. In order to transform the tan-

gential coordinate  $\varphi$ , we also had to subtract the component reflecting its monotonic growth. In effect the following values were transformed:  $v_r$ ,  $r - (\Sigma r^i)/N$ ,  $v_t - (\Sigma v_t^i)/N$ ,  $\varphi_c - (\Sigma \varphi_c^i)/N$ , where  $\varphi_c = \varphi - \bar{\Omega}t$ ,  $t$  is the time since the moment when the particle started,  $\bar{\Omega} = (\varphi^N - \varphi^1)/T$ , and  $T$  is the total time for which the particle has been traced. The sum  $\Sigma$  is over all  $N$  samplings, and the upper index counts the samplings. Moreover, the angular coordinate  $\varphi$  and the tangential velocity  $v_t$  were transformed for the frame of reference of each bar ( $\varphi_{c1}$ ,  $\varphi_{c2}$  and  $v_{t1}$ ,  $v_{t2}$ ), hence 6 dynamical variables were transformed in total.

In Fig.3, we present one-sided power spectral density (for brevity called here power spectra) from fast Fourier transform for each variable on an exemplary regular trajectory. They are essentially line spectra, as most of the power resides in a few separated peaks. Note the quality of the spectra: the power density in the peaks is several orders of magnitude higher than that in the baseline. Power spectra of all six dynamical variables transformed have the same distribution and similar strengths of major peaks. Only spectra of the angular coordinate  $\varphi$  are of slightly lower quality, with higher baseline, and power increasing towards the lowest frequencies. This is likely the effect of inaccuracies in double corrections applied to the measured value of those variables. Even in these spectra, however, the peaks are at least two orders of magnitude in power over the highest values of the baseline. In the rest of this paper, we focus on the analysis of the spectrum of the radial coordinate only, for which our Fourier algorithm returns data of best quality.

### 4.2.1 Most regular trajectory as a double-frequency orbit

In Fig. 4, we present power spectra for the three trajectories from Figures 1 and 2. We display the power density in both the linear scale (left panels), and the logarithmic scale (right panels). The power spectrum for the most regular trajectory from Fig.2 is shown in the top row. It shows sharp peaks at two frequencies:  $\omega_2 = 163.7 \text{ km s}^{-1} \text{ kpc}^{-1}$  and  $\omega_1 = 199.4 \text{ km s}^{-1} \text{ kpc}^{-1}$ . These peaks contain about 95% of total spectral power. Most of the remaining power is in secondary peaks at frequencies which are functions of  $\omega_1$  and  $\omega_2$ , namely  $\omega_1 + \omega_2$ ,  $2\omega_1$ ,  $2\omega_2$ ,  $\omega_2 - \omega_1$  etc. The power in the secondary peaks rapidly decreases as a function of their frequency: the group of three peaks between 300 and 400  $\text{km s}^{-1} \text{ kpc}^{-1}$  contains less than 2% of the total power, and further peaks contain still one order of magnitude less of the total power.

The two frequencies,  $\omega_1$  and  $\omega_2$ , at which almost all of the power resides, are separated by  $35.75 \text{ km s}^{-1} \text{ kpc}^{-1}$ . This is exactly twice  $\Omega_2 - \Omega_1$ , the difference between the pattern speeds of the bars in Model 1. In Sect.3, we showed that in the linear approximation the solution for the radial coordinate (17) of a particle moving in the potential of two independently rotating bars, in the absence of free oscillations, consists of two oscillations with frequencies  $\omega_1$  and  $\omega_2$  defined by (11). The difference between those frequencies is also  $2(\Omega_2 - \Omega_1)$ . Thus, we imply that the frequencies of the highest peaks in the power spectrum of the trajectory from Fig.2 are in fact the frequencies of driving by the two bars, and that they are nonlinear equivalents of the  $\omega_i$ 's defined by (11). From (11) one can obtain the underlying orbital frequency of the particle:  $\Omega = 123.75 \text{ km s}^{-1} \text{ kpc}^{-1}$ . It is close to its epicyclic approximation at the guiding radius  $r_0 = (\Sigma r^i)/N = 1.803 \text{ kpc}$ , which is  $121.5 \text{ km s}^{-1} \text{ kpc}^{-1}$ . This consistency further confirms our finding. Thus in both the linear case (epicyclic approximation) and in the general case, we constructed double-frequency orbits in an oscillating potential of a double bar, with frequencies equal to

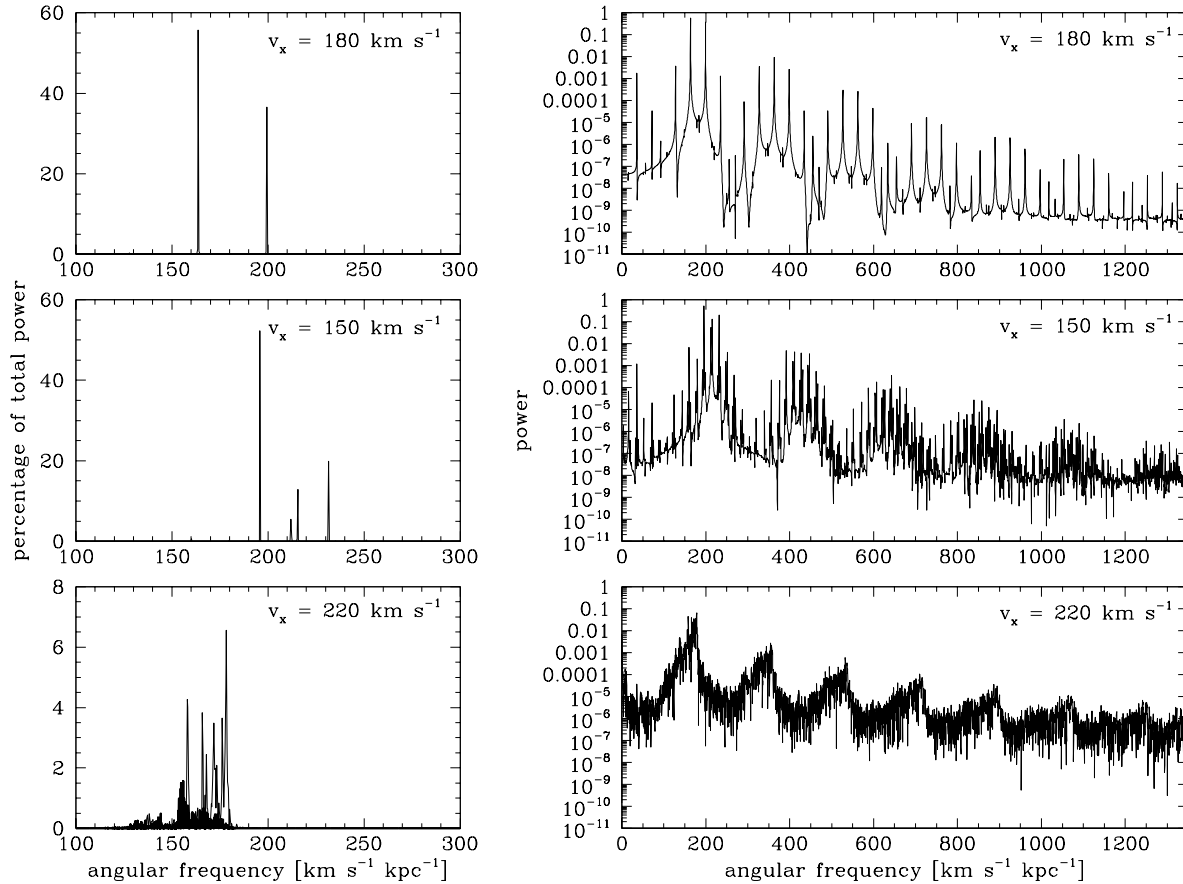


**Figure 4.** Power spectra of the radial coordinate on three representative trajectories, shown in linear (left-hand panels) and logarithmic (right-hand panels) scale. The plots in the top row show the power spectrum of the double-frequency orbit from Fig.2. The plots in the middle and bottom rows show, respectively, power spectra of the trajectories from the right-hand and left-hand panels of Fig.1. The particle was followed for 100 relative periods of the bars, with dynamical variables sampled  $N = 2^{13}$  times at equal time intervals. In the bottom-left panel, the thick line marks an additional power spectrum, for the same initial conditions, but with the particle followed for 600 relative periods of the bars, with dynamical variables sampled  $N = 2^{16}$  times.

the frequencies of driving by the bars. Note that since the Fourier analysis requires the particle to be followed for many relative periods of the bars, and since no fine adjustments of initial conditions were made, this double-frequency orbit is most likely stable.

#### 4.2.2 Trajectory trapped around double-frequency orbit

Below, we will show that the trajectory from the right panels of Fig.1 involves free oscillation in addition to the two oscillations driven by the bars. The power spectrum for this trajectory is shown in the middle row of Fig.4. It shows four major peaks. The two highest peaks at  $\omega_2 = 195.9 \text{ km s}^{-1} \text{ kpc}^{-1}$  and  $\omega_1 = 231.7 \text{ km s}^{-1} \text{ kpc}^{-1}$  are separated by twice the difference between the pattern speeds of the bars,  $2(\Omega_2 - \Omega_1)$ , which indicates that they occur at the frequencies of oscillations driven by the bars. Again, from (11) one can obtain the underlying orbital frequency of the particle:  $\Omega = 139.8 \text{ km s}^{-1} \text{ kpc}^{-1}$ , and from averaging the radial coordinate one can get an approximation for the guiding radius  $r_0 = 1.579 \text{ kpc}$ . In the linear approximation, the orbital frequency at this guiding radius is  $137.5 \text{ km s}^{-1} \text{ kpc}^{-1}$ , again consistent with the nonlinear solution. About 70% of the total power resides in these two peaks at frequencies of the driving by the two bars.

Between the two highest peaks in the power spectrum, there are two other peaks of lower amplitude. They are located at fre-

quencies  $\kappa = 211.9 \text{ km s}^{-1} \text{ kpc}^{-1}$  and  $\kappa' = 215.5 \text{ km s}^{-1} \text{ kpc}^{-1}$ , which are not commensurate with  $\omega_1$  and  $\omega_2$ , and they contain about 20% of the total power. Note that  $\omega_1 - \kappa' = \kappa - \omega_2$ , which means that  $\kappa$  and  $\kappa'$  are not independent, and therefore that these two peaks indicate only one additional frequency on the trajectory. We postulate that this frequency is the free oscillation frequency. In the linear approximation of Sect.3, this frequency corresponds to  $\kappa_0$  in (17), which for the guiding radius  $r_0 = 1.579 \text{ kpc}$  is equal to  $202 \text{ km s}^{-1}$ . This value is somehow different from  $\kappa$  and  $\kappa'$  measured in the power spectrum, but it remains in their vicinity. Moreover, qualitatively one should expect that at this guiding radius  $\kappa$  and  $\kappa'$  lie in between  $\omega_1$  and  $\omega_2$ , because in the linear approximation  $\Omega - \kappa/2$  takes values between  $\Omega_1$  and  $\Omega_2$  there.

All other peaks in the spectrum occur at frequencies which are functions of  $\omega_1$ ,  $\omega_2$  and  $\kappa$ , and power contained in those peaks decreases rapidly with frequency. Thus it appears that the orbit from the right panels of Fig.1 is trapped around a double-frequency orbit and oscillates around it with the characteristic frequency  $\kappa$ .

#### 4.2.3 Chaotic trajectory

Finally, the power spectrum of the trajectory from the left panels of Fig.1 is shown in the bottom rows of Fig.4. There are more peaks, and also much power contained in between the peaks. In order to

validate the significance of the peaks in this spectrum, we calculated again power spectra for the three trajectories from Figs. 1 and 2, but now followed for 600 alignments of the bars, with dynamical variables recorded at  $2^{16}$  equal time intervals. While the power spectra for the two trajectories analyzed above do not show significant changes, the new spectrum for the trajectory from the left panels of Fig.1, marked with the thick line in the bottom-left panel of Fig.4, shows multitude of peaks, each of them containing no more than 2% of the total power. Kandrup, Eckstein & Bradley (1997) showed that a multitude of frequencies indicates chaos (see also Athanassoula 2005). In the case analyzed here, there is a continuous distribution of power with broad maximum in the frequency range between 120 and 190  $\text{km s}^{-1} \text{ kpc}^{-1}$ . Such a power spectrum is characteristic of a chaotic trajectory.

### 4.3 The vicinity of a double-frequency orbit

In order to study how particles get trapped around double-frequency orbits, one can explore a range of initial conditions around the ones that characterize it. We developed an automatic procedure that finds local maxima (peaks) in the power spectrum at frequencies  $\omega_1$  and  $\omega_2$  corresponding to the driving by the two bars and at the free oscillation frequency. We based this procedure on the fact that the two frequencies of driving by the two bars are always separated by  $2(\Omega_2 - \Omega_1)$ , where  $\Omega_1$  and  $\Omega_2$  are the (constant) pattern speeds of the two bars. Thus, the algorithm first searches for the highest peak in the power spectrum, and records its frequency  $\omega$ . Then it examines power spectrum at frequencies  $\omega \pm 2(\Omega_2 - \Omega_1)$ . If there is a peak in one of these frequencies, then this frequency and  $\omega$  are recorded as  $\omega_1$  and  $\omega_2$  on this orbit, as defined in (11). Furthermore, the free oscillation frequency  $\kappa$  is found by searching for the peak with highest power that does not occur at a frequency which is a linear combination of  $\omega_1$  and  $\omega_2$ .

In our analysis, we kept focus on a particle that starts at the 1.7-kpc distance from the galaxy centre, on the minor axis of the aligned bars, with its initial velocity perpendicular to that axis. We analyzed a range of values of the initial velocity between 130  $\text{km s}^{-1}$  and 230  $\text{km s}^{-1}$ . The initial conditions for the three trajectories studied above fall within this range. The dotted line in the upper panel of Fig.5 indicates the average radius  $r_0 = (\Sigma r^i)/N$  (where the meaning of the symbols is the same as in Sect.4.2) as a function of the initial velocity  $v_x$ . As expected, higher initial velocity results in larger average radius, although the relation becomes not monotonic and noisy at initial velocities above 205  $\text{km s}^{-1}$ . When the average radius is taken as the radius of the guiding centre in the linear approximation, one can calculate the orbital frequency  $\Omega$  and the free oscillation frequency  $\kappa$  in this approximation. They are drawn in thick solid and dashed lines, respectively.

On the other hand, once we derive  $\omega_1$  and  $\omega_2$  from the power spectrum of the trajectory, the orbital frequency  $\Omega$  in the full non-linear solution can be obtained from (11). The values of  $\Omega$  derived from the measured values of  $\omega_1$  and  $\omega_2$  are the same, and they are plotted with a thin solid line in the upper panel of Fig.5. They closely follow the values derived in the linear approximation for most of the range, although there are clear departures at initial velocities above 205  $\text{km s}^{-1}$ . Although our algorithm to analyse the power spectrum allows us to extract automatically the free oscillation frequency  $\kappa$ , one should also expect a peak at  $\kappa' = \omega_1 + \omega_2 - \kappa$ , because two frequencies,  $\omega_1$  and  $\omega_2$ , are already present in the system. In fact, the algorithm finds peaks at two frequencies  $\kappa$  and  $\kappa'$ , whose sum is  $\omega_1 + \omega_2$ . Both of these frequencies are drawn in the upper panel of Fig.5 (thin dashed lines), since from the power

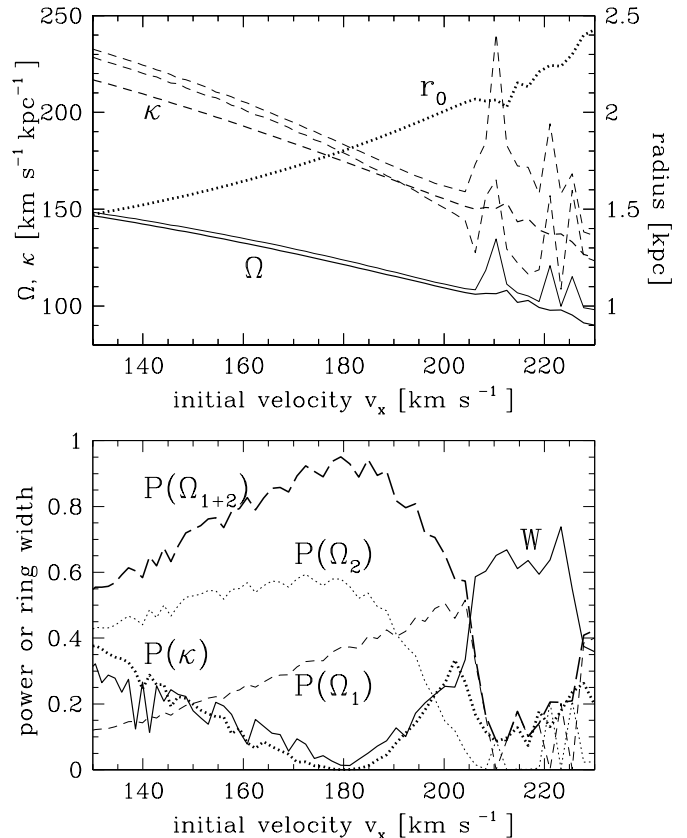


**Figure 5.** Parameters that characterize orbits in Model 1 by Maciejewski & Sparke (2000), which start at 1.7-kpc distance from the galaxy’s centre, on the minor axis of the bars when the bars are aligned, and with a velocity vector at right angle to it, plotted as a function of the magnitude of the starting velocity  $v_x$ . *Upper panel:* Thick dotted line marks the average radius of the orbit,  $r_0 = (\Sigma r^i)/N$ . The epicyclic approximation for the angular frequency  $\Omega$  and for the frequency of free oscillations  $\kappa$  at this radius are plotted with thick solid and dashed lines, respectively. The values of  $\Omega$  and  $\kappa$  derived from the power spectrum of the orbit are plotted with thin solid and dashed lines, respectively. *Lower panel:* Percentage of the total power residing at the frequencies of the major peaks. The thin dashed line marks the power  $P(\Omega_1)$  at the driving frequency of the outer bar, and the thin dotted line marks  $P(\Omega_2)$  at the driving frequency of the inner bar. The sum of  $P(\Omega_1)$  and  $P(\Omega_2)$ ,  $P(\Omega_{1+2})$ , is plotted with a thick dashed line. The thick dotted line marks the power  $P(\kappa)$  in the two peaks arising from the free oscillation frequency. The thick solid line marks the median width of the ring enclosing particle positions at consecutive alignments of the bars, in units of the average radius of the orbit  $r_0$  (see Sect.4.4).

spectrum one cannot determine which one is the actual  $\kappa$ . Their functional dependence on the initial velocity  $v_x$  is similar to that obtained in the linear approximation, although the slope is slightly different, and the quantitative discrepancy is larger than in the case of the orbital frequency  $\Omega$ . Again,  $\kappa$  and  $\kappa'$  as a function of the initial velocity become ragged for  $v_x > 205 \text{ km s}^{-1}$ .

One can also examine how much of the total power resides in various peaks in the Fourier spectrum. In the lower panel of Fig.5, a thin dashed line indicates the power  $P(\Omega_1)$  residing in the peak at the frequency of driving by the outer bar, while a thin dotted line indicates the power  $P(\Omega_2)$  in the peak at the frequency of driving by the inner bar. With the thick dashed line we plotted the power  $P(\Omega_{1+2})$  residing in both peaks above. Power  $P(\kappa)$ , residing in the two peaks related to the free oscillation frequency,



is plotted with a thick dotted line. From the plot one can see that in the range of initial velocity  $v_x$  between  $130 \text{ km s}^{-1}$  and  $205 \text{ km s}^{-1}$ ,  $P(\Omega_{1+2})$  and  $P(\kappa)$  sum up roughly to 100%. This means that only three frequencies are present on those trajectories, as expected for the regular orbits (see Sect.2). In this range, the larger the value of  $P(\kappa)$ , the smaller  $P(\Omega_{1+2})$ . However, throughout this range  $P(\Omega_{1+2}) > 0.5$ , which means that more than half of the total power is located in the two peaks at the driving frequencies of the two bars. Orbits with larger average radii  $r_0$  have more power in the driving frequency of the outer bar, while orbits with smaller  $r_0$  have most of their power in the driving frequency of the inner bar. For  $v_x$  around  $180 \text{ km s}^{-1}$ , up to 95% of the total power resides at the driving frequencies of the two bars, and only 0.03% in the free oscillations. Thus the trajectory with  $v_x$  around  $180 \text{ km s}^{-1}$  is made up almost entirely of oscillations with the driving frequencies of the two bars. This is the double-frequency orbit from Fig.2. The more  $v_x$  differs from  $180 \text{ km s}^{-1}$ , the larger fraction of the total power resides in the free oscillations: up to 38% and 33% at  $v_x = 130 \text{ km s}^{-1}$  and  $v_x = 202 \text{ km s}^{-1}$ , respectively. This is typical for trajectories trapped around stable regular orbits. An example of such a trajectory is the one from the right panels of Fig.1, for which  $v_x = 150 \text{ km s}^{-1}$ .

For  $v_x > 205 \text{ km s}^{-1}$ , the summed power in peaks related to the three frequencies considered here is far smaller than 100%. The initial conditions of the trajectory from the left panels of Fig.1 belong to this range of  $v_x$ . The power spectrum of that trajectory (Fig.4, bottom row) shows the power distributed in a continuum of frequencies, which is characteristic for a chaotic orbit. Thus trajectories with  $v_x > 205 \text{ km s}^{-1}$  are most likely chaotic. This explains the noise for  $v_x > 205 \text{ km s}^{-1}$  in the curves that mark the frequencies derived from Fourier analysis in the top panel of Fig.5. One can point out the region of onset of chaos at  $v_x$  between  $200 \text{ km s}^{-1}$  and  $210 \text{ km s}^{-1}$ , where both  $P(\Omega_{1+2})$  and  $P(\kappa)$  drop sharply with  $v_x$ .

#### 4.4 Construction of loops from double-frequency orbits

In the epicyclic approximation, the double-frequency orbits have a nice feature, namely that particles following them populate loops: closed curves that return to their original shape and position at every alignment of the bars. One may therefore expect that also in the general case considered here particles on double-frequency orbits populate loops. In order to check, whether it is the case, we follow the same procedure as in the epicyclic approximation. We start a particle from the minor axis of the aligned bars, and record its position and velocity every time the bars align again. Let  $x_0$  mark the starting position and velocity of the particle,  $x_1$  its position and velocity at the first consecutive alignment of the bars and so on. Positions of a particle on a double-frequency orbit are overplotted in Fig.2 for the first 20 alignments of the bars. In the left panel of Fig.6, we plotted 60 positions for 60 alignments. They seem to be arranged on a closed curve of oval shape.

Let us now take  $N$  values of  $x_i$  as initial conditions for a set of  $N$  particles at one alignment of the bars. By construction, a particle starting at  $x_i$  will be located at  $x_{i+1}$  at the next alignment of the bars. Thus, if positions of a particle at every alignment of the bars populate a closed curve, this curve will transform into itself every time the bars align. This is what we defined as a loop. In the left panel of Fig.6 one can see that positions of a particle on a double-frequency orbit, written at every alignment of the bars, populate a closed curve, which is a loop. Therefore, one may expect that the relation between double-frequency orbits and loops found in the

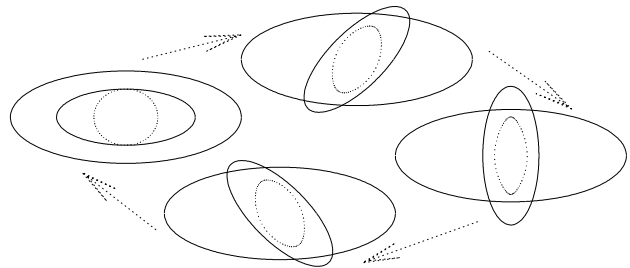


**Figure 6.** *Left panel:* Positions of a particle on the double-frequency orbit from Fig.2 at consecutive alignments of the bars generate a loop. Here 60 positions are recorded. *Remaining panels:* Evolution of the loop during one relative period of the bars. The bars, outlined with solid lines, rotate counterclockwise.

linear approximation also holds in the general case. Note that this construction of a loop requires the particle to be followed for many relative periods of the bars, hence it will likely produce loops that are maps of stable double-frequency orbits only.

The loop returns to its original shape and position at every alignment of the bars. Recording positions of particles from the loop at any time between alignments of the bars will unveil how the loop evolves between the alignments. This has been shown in the remaining panels of Fig.6, where we plotted locations of these particles at three other relative positions of the bars. The particles remain confined to the loop, but the shape of the loop varies in between the alignments.

Will particles on other orbits, which involve free oscillations, take any particular positions at every alignment of the bars? One may expect that since such orbits oscillate around double-frequency orbits, the recorded positions will gather around the loop. If so, they should be enclosed within a band of certain width that increases with the amplitude of free oscillation. This band, surrounding the loop, is closed and, following the notation introduced by Maciejewski & Sparke (2000), we will call it the ring. In order to see how the width of the ring changes with the amplitude of free oscillation, we applied the following algorithm, similar to the one used by Maciejewski & Sparke (2000). We registered particle positions on the orbit at 400 alignments of the bars. We divided the full  $2\pi$  angle into 80 equal parts, and for each part we calculated the range  $\Delta r$  of radii among the positions falling into this part. The median of the  $\Delta r$  values is taken as the estimate of the ring width  $W$ .

In the bottom panel of Fig.5 we plot the ring width  $W$ , normalized to the average radius of the orbit  $r_0$ , as a function of the starting velocity. At velocities between  $130 \text{ km s}^{-1}$  and  $200 \text{ km s}^{-1}$ , the ring width  $W$  is below 30% of the average radius, hence recorded positions occupy a well defined ring. The ring gets thinner for velocities close to  $180 \text{ km s}^{-1}$ . This is the initial condition for the double-frequency orbit from Fig.2 that generates the loop from Fig.6. For this orbit  $W$  is about 2%. Generally, in the range of initial velocities considered here,  $W$  behaves in a very similar way to  $P(\kappa)$ . The larger the free oscillations around the double-frequency orbit, the wider the ring enclosing recorded positions. Therefore, we confirm our expectations that orbits trapped around double-frequency orbits map onto rings surrounding the loop.

Note that in this algorithm,  $W$  is zero only for circular loops or under infinitely fine sampling in angle. Otherwise,  $W$  is only near zero for a loop. However, unlike the amplitude of free oscillation with frequency  $\kappa$ ,  $W$  is very straightforward to measure and to visualize. The excellent agreement between the functional behaviour

of  $W$  and  $P(\kappa)$  exemplified in Fig.5 makes  $W$  a useful indicator of a loop.

For initial velocities between  $200 \text{ km s}^{-1}$  and  $210 \text{ km s}^{-1}$  the median ring width sharply rises from 30% to 70% of the average radius. Such large median width indicates that recorded positions are no longer confined by a ring, but rather densely populate some fraction of the plane, and do not gather on any curve. This is characteristic for chaotic orbits, which is consistent with the frequency analysis above.

## 5 DISCUSSION AND CONCLUSIONS

The goal of this paper is to present an argument that the backbone of an oscillating potential of a doubly barred galaxy is built out of double-frequency orbits. In Sect.3, by using the linear approximation, we showed that two frequencies are indispensable in motion in such systems. A single frequency, and thus a closed periodic orbit, can occur only when these two frequencies are commensurate. However, even in such case they are two separate frequencies, which happen to have the same numerical value. This is a condition for resonance, like the one in the single bar when the frequency of free oscillations is equal to that of driving by the bar.

Double-frequency orbits in the oscillating potential of double bars do not close. Their appearance is also different in the reference frame of each bar. However, their perception and analysis is facilitated greatly by the fact that they map onto loops, which are closed curves. The mapping is done by recording the positions on the orbit at every alignment of the bars. In such a construction, points that are on the loop will remain on the loop. A loop can be viewed as a set of particles, and therefore its appearance is independent from the frame of reference. However, the loop oscillates in time with a period equal to the relative period of the bars.

In the linear approximation we showed rigorously that each double-frequency orbit maps onto a loop. In the general, non-linear case, we found that when the Fourier analysis of the orbit indicates almost all power at the frequencies of driving by the bars, and almost no power at the free oscillation frequency, the map of the orbit is to a good approximation a 1-D curve. This is the loop. When free oscillations are present, the orbit maps onto a set of points in a ring surrounding the loop. The width of this ring is higher when more power is in the free oscillations.

From the power spectrum of an orbit in the oscillating potential of a doubly barred galaxy we can retrieve its three fundamental frequencies (frequencies of forcing by the two bars and the frequency of free oscillations) when the orbit is regular. Otherwise a continuous power spectrum is recovered when the orbit is chaotic. The Fourier algorithm that we apply displays the baseline at no more than  $10^{-4}$  of the total power, hence peaks higher than that can be easily extracted. Thus, even if the power in e.g. the free oscillation is very small around the loop, our algorithm recovers its frequency correctly, as the continuity of the  $\kappa(v_x)$  curve in the top panel of Fig.5 indicates. In our algorithm, the power spectrum of each trajectory is analyzed independently from power spectra of neighbouring trajectories, and frequencies recovered on one trajectory do not enter as an ‘initial guess’ for those on the nearby trajectory. Therefore, continuity of  $\Omega$  and  $\kappa$  as functions of the initial velocity  $v_x$  is a genuine property of the system, and not of the algorithm.

Methods employed in this paper in the search for double-frequency orbits and loops require the particle to be followed for many (i.e. hundreds) relative periods of the bars. We do not perform

fine tuning of the initial conditions on the trajectory, hence recovering unstable orbits with these methods is rather unlikely. Therefore double-frequency orbits recovered with the methods employed in this paper are stable in the sense that they trap regular orbits, which wind tightly around them and map onto rings enclosing loops.

We conclude that in a potential of two independently rotating bars, regular trajectories are trapped around parent stable double-frequency orbits. They oscillate around these orbits, like trajectories in a single bar oscillate around stable closed periodic orbits. The two frequencies present on the parent orbits correspond to the frequencies of driving by the two bars. Therefore the parent orbits do not close in any reference frame. However, they can be mapped onto the loops, whose appearance is independent from the reference frame. As such, loops are a unique tool that greatly facilitates the search for regular orbits in oscillating potentials.

**Acknowledgments.** This work was carried out within the framework of the European Associated Laboratory ‘‘Astrophysics Poland-France’’. It was supported by the Polish Committee for Scientific Research as a research project 1 P03D 007 26 in the years 2004–2007. WM thanks the CNRS for an associate position, which made this collaboration possible.

## REFERENCES

- Athanassoula, E., 1992, *MNRAS*, 259,328  
Athanassoula, E., 2005, in ‘‘Nonlinear Dynamics in Astronomy and Physics (In memory of Henry E. Kandrup)’’, eds. S. T. Gottesman, J.-R. Buchler and M. E. Mahon, *Annals of the New York Academy of Sciences*, 1045, 168  
Binney, J., Spergel, D., 1982, *ApJ*, 252, 308  
Binney, J., Spergel, D., 1984, *MNRAS*, 206, 159  
Binney, J., Tremaine, S., 1987, *Galactic Dynamics*. Princeton Univ. Press, Princeton  
Broucke, R.A., 1969, *Periodic Orbits in the Elliptic Restricted Three-Body Problem*, Jet Propulsion Laboratory Report 32-1360  
Buta, R., Crocker, D.A., 1993, *AJ*, 105, 1344  
Debattista, V.P., Shen, J., 2007, *ApJ*, 654, L127  
El Zant, A., Shlosman, I., 2002, *ApJ*, 577, 626  
Erwin, P., 2004, *A&A*, 415, 941  
Erwin, P., Sparke, L.S., 2002, *AJ*, 124, 65  
Friedli, D., Martinet, L., 1993, *A&A*, 272, 27  
Friedli, D., Wozniak, H., Rieke, M., Martinet, L., Bratschi, P., 1996, *A&AS*, 118, 461  
Heller, C., Shlosman, I., Athanassoula, E., 2007, *ApJL*, 657, L65  
Howard, G., 1994, M.S. Thesis, Univ. Wisconsin–Madison  
Kandrup, H. E., Eckstein, B. L., Bradley, B. O., 1997, *A&A*, 320, 65, 1997  
Laine, S., Shlosman, I., Knapen, J.H., Peletier, R.F., 2002, *ApJ*, 567, 97  
Lichtenberg, A.J., Leiberman, M.A., 1992, *Regular and Chaotic Dynamics*, 2nd edition. Springer, New York  
Louis, P.D., Gerhard, O.E., 1988, *MNRAS*, 233, 337  
Maciejewski, W., Sparke, L.S., 1997, *ApJL*, 484, L117  
Maciejewski, W., Sparke, L.S., 2000, *MNRAS*, 313, 745  
Rautiainen, P., Salo, H., Laurikainen, E., 2002, *MNRAS*, 337, 1233  
Sridhar, S., 1989, *MNRAS*, 238, 1159  
Wozniak, H., Friedli, D., Martinet, L., Martin, P., Bratschi, P., 1995, *ApJS*, 111, 115